Bifurcation and Catastrophe in a Simple, Forced, Dissipative Quasi-Geostrophic Flow

JAMES G. VICKROY AND JOHN A. DUTTON[1]

Department of Meteorology, The Pennsylvania State University, University Park 16802

(Manuscript received 21 November 1977, in final form 28 September 1978)

ABSTRACT

The steady solutions and their stability properties are investigated for a low-order spectral model of a forced, dissipative, nonlinear, quasi-geostrophic flow. A zonal flow is modified by two smaller scale disturbances in the model.

If only the zonal component (or only the smallest scale component) is forced, then the stationary solution is unique, always locally stable, and globally stable for weak forcing.

There is also a unique locally stable stationary solution for weak forcing of only the middle component. But as this forcing exceeds a critical value, a supercritical bifurcation to new solutions appears.

The entire solution surface for forcing of the zonal and middle components can be displayed graphically and is a form of the well-known cusp catastrophe surface. For forcing of all three components, the morphogenesis set is more complex, containing regions in which there are one, three or five solutions.

Numerical integrations of the phase-space trajectories of the solutions reveal that for forcing of the zonal and middle components 1) domains of attraction of stable steady solutions contain neighborhoods near the unstable steady solution, 2) there is a region near the cusp in which initial points produce periodic solutions, and 3) initial points further away from the cusp yield trajectories that quickly approach stable steady solutions.

The conclusion is that any successful theory of atmospheric climate will have to contend with multiple solutions and changing domains of attraction as external parameters are varied.

1. Introduction

Nonlinearity is an essential part of atmospheric processes ranging from turbulence to climatic evolution, as is manifest because the distribution of kinetic energy with wavelength can only evolve through nonlinear interactions. The consequence is that nonlinearity and its effects have important implications in the study of predictability, frontal processes, climate theory, and other topics of current interest and importance.

The purpose of this paper is to investigate a particular aspect of the nonlinear behavior of large-scale flows using a prototype model developed from the quasi-geostrophic equation. Specifically, we emphasize stationary solutions of the heated, dissipative problem, and demonstrate the existence of nonunique (or multiple) solutions of the kind found in the developing mathematical speciality known as bifurcation and catastrophe theory.

The quasi-geostrophic equation was developed by Charney (1947), who combined the observations that large-scale midlatitude flow is nearly hydrostatic, geostrophic and wavelike with scale analysis to produce a partial differential equation for a streamfunction. The equation contains the advective nonlinearity responsible for kinetic energy transfers among wavelengths and represents a compromise between the complexities of the Navier-Stokes equations and the simplicity necessary for rigorous and explicit results to be obtained.

Properties of the quasi-geostrophic equation (or similar vorticity conservation equations) have been studied by Fjørtoft (1953), Lorenz (1960), Platzman (1960, 1962), Baer (1970), Charney (1971) and Dutton (1974, 1976a). It was demonstrated (Dutton, 1974) that the initial value problem for unforced, inviscid flow has unique solutions on a bounded domain, and that the truncated spectral solutions are almost always recurrent on the hyper-ellipsoid representing a constant energy surface.

A direct Newtonian heating mechanism of the kind used by several authors (including Fjørtoft, 1959; Dickinson, 1969; Stone, 1972) was added to the equation by Dutton (1976a) along with a direct dissipation mechanism. The consequence was that the truncated spectral solutions then progress inexorably toward a region of phase space in which they are all eventually confined. This property of forced, dissipative, hydrodynamic spectral models was demonstrated by Lorenz (1960).

In this paper we turn to a study of the stationary solutions of the truncated spectral equations, and we adopt the philosophy proposed in Lorenz (1960, 1963)

[1] Current affiliation: Visiting Scientist, Risø National Laboratory, Denmark.

0022-4928/79/010042-11$06.75

that essential aspects of the physics of complex hydrodynamic systems are revealed by models that are simplified to the point of containing the nonlinearity in its most basic manifestation. Thus, we shall study a severely truncated spectral model containing a zonal flow and two disturbance components that interact nonlinearly. Such a model is the simplest form that resembles the synoptic structure of midlatitudes.

The existence of stationary solutions for arbitrarily large spectral models was demonstrated by Dutton (1976a); in low-order models they may be specified algebraically, but usually numerical techniques will be necessary to find them explicitly. Analysis of the detailed mathematical structure of the flows specified by the spectral equations necessarily begins with a knowledge of the stationary solutions and of the behavior of perturbations superimposed on them.

The most striking consequence of the nonlinearity of the problem is that the nature of the stationary solutions can change dramatically as the parameters governing the problems are changed. Most significantly, stable solutions become unstable and there are combinations of the parameters for which multiple solutions appear.[2]

These phenomena are studied in the mathematical specialty of bifurcation and catastrophe theory (Stakgold, 1971; Thom, 1976; Zeeman, 1976). In bifurcation a solution becomes unstable at the point that new solutions branch away from it. This behavior has long been studied in hydrodynamics, with the bifurcation or branching representing the loss of stability of a basic solution when the physical process then proceeds to a new stable situation. In catastrophe theory, the situation is different because there may not be branching, but rather sudden appearance or disappearance of a solution. For example, as a determining parameter is increased past a critical value, a basic solution will cease to exist or suddenly appear. This situation appears to be the origin of the name catastrophe, for a mathematical and physical catastrophe does occur at that point. A real process may undergo a dramatic change at the point the critical value was surpassed.

We analyze a three-coefficient model (the most complex one that permits graphical display of the solution surface) and shall show that its solution surfaces are typical of those encountered in catastrophe theory. When only two of the three components are forced, we find a cusp catastrophe explicitly.

These results are the first demonstration of which we know that the behavior predicted by catastrophe theory appears in atmospheric dynamics. The consequences—some startling and some in agreement with our intuition and experience with atmospheric flow—are further evidence of the profound effect of nonlinearity in shaping meteorological events.

2. A spectral model for quasi-geostrophic flow

The nonlinear quasi-geostrophic equation for conservative horizontal flow[3] is

$$\frac{\partial}{\partial t}(\nabla_H^2\psi)+J(\psi,\nabla_H^2\psi)+\beta\frac{\partial\psi}{\partial x}=0. \tag{2.1}$$

in which ψ is the nondimensional streamfunction and the Jacobian operator is defined as

$$J(f,g)=\frac{\partial f}{\partial x}\frac{\partial g}{\partial y}-\frac{\partial f}{\partial y}\frac{\partial g}{\partial x}. \tag{2.2}$$

The β-plane approximation is used so that the Coriolis parameter is $f=f_0+\beta y$, where subscripts denote independence of latitude. Recent analyses of the ranges of validity of this equation may be found in Phillips (1963) or Dutton (1976b).

We choose to circumvent the difficulties of representing the range of scales involved in the actual physical process of transferring energy to eddies for dissipation by using a direct dissipation mechanism $\nu\nabla_H^4\psi$ (Dutton, 1976a) in which the eddy viscosity coefficient ν is constant. The forcing will be a simplified form of Newtonian heating in which $H=\partial Q/\partial z|_{zL}$ is calculated from $Q\propto\theta_e-\theta_0$ at the level z_L at which (2.1) applies. The heating term derives from the first law of thermodynamics. Details and notation are given in Dutton (1976a). The model is then specified by

$$\frac{\partial}{\partial t}(\nabla_H^2\psi)+J(\psi,\nabla_H^2\psi)+\beta\frac{\partial\psi}{\partial x}=H+\nu\nabla_H^4\psi. \tag{2.3}$$

The quasi-geostrophic equation was developed to model conditions prevalent in midlatitudes, and we apply it here to a channel flow that is analogous to a westerly current centered at 45°N.

Appropriate boundary constraints on ψ for such a channel are 1) periodicity in the east–west direction, 2) the meridional velocity component v vanishes along the northern and southern boundaries, and 3) no circulation may develop around the boundaries so that

$$\int_x \frac{\partial^2\psi}{\partial t\partial y}\bigg|_{y\ \text{boundary}} dx=0$$

[2] Note the difference between nonuniqueness in this case and uniqueness in the initial value problem. Here we are letting the governing parameters vary, and finding multiple stationary solutions for some combinations. In the initial value problem, the parameters are fixed, and we consider the temporal behavior of solutions starting from a specified initial point.

[3] The fact that the spectral equations are identical in form for horizontal and baroclinic quasi-geostrophic flows was shown by Baer (1970), and is evident from the fact that the expansion of the vertical structure adds coefficients but does not change the character of the spectral equations.

(Phillips, 1954). For simplicity, we make no attempt to specify lateral boundary conditions consistent with the effects of viscosity on either rigid or free surfaces.

To develop the spectral model, we solve $\nabla_H^2\psi = -\lambda_n\psi$ and then use the solutions ψ_n to write

$$\psi = \sum_{n=1}^{N} a_n(t)\psi_n. \tag{2.4}$$

The spectral representation of the quasi-geostrophic model is obtained by substituting (2.4) in (2.3), multiplying (2.3) by ψ_n, and integrating over the spatial domain D for each $n=1, 2, \ldots, N$. Because the ψ_n are orthogonal we obtain

$$\lambda_n \frac{\partial}{\partial t} a_n + \sum_{k=1}^{N}\sum_{m=1}^{N} \lambda_m D_{kmn} a_k a_m - \sum_{j=1}^{N} \beta C_{jn} a_j = -H_n - \nu\lambda_n^2 a_n, \tag{2.5}$$

where

$$D_{kmn} = \int_D \psi_n J(\psi_k, \psi_m) d\mathbf{x},$$

$$C_{jn} = \int_D \psi_n \frac{\partial \psi_j}{\partial x} d\mathbf{x},$$

$$H_n = \int_D \psi_n H(\mathbf{x}) d\mathbf{x}.$$

The stationary solutions will involve N coefficients a_n as functions of N heating rate parameters H_n. Thus the description of the dependence of one coefficient on the H_n will require $N+1$ dimensional geometry. The most complex picture that we can draw, therefore, is the response of a single coefficient to two heating parameters. Thus for this initial investigation, in which we wish to have an explicit graphical portrayal of results, we shall choose a three-coefficient model, and much of the time set one heating rate to zero. Thus we put

$$\psi(\mathbf{x},t) = a_1(t)\frac{\sin(y)}{\pi} + a_2(t)\frac{\sqrt{2}\cos(y)\sin(lx)}{\pi} + a_3(t)\frac{\sqrt{2}\cos(3y)\cos(lx)}{\pi}, \tag{2.6}$$

where

$$D = \left\{x: 0 \leqslant x \leqslant 2\pi,\ y: -\frac{\pi}{2} \leqslant y \leqslant \frac{\pi}{2}\right\}.$$

The eigenvalues are $\lambda_1=1$, $\lambda_2=1+l^2$, $\lambda_3=9+l^2$.

With this choice, the model equations become

$$\left.\begin{aligned} \dot{a}_1 + [(\lambda_3-\lambda_2)/\lambda_1]D_{231}a_2a_3 + \nu\lambda_1 a_1 &= -H_1/\lambda_1 \\ \dot{a}_2 + [(\lambda_1-\lambda_3)/\lambda_2]D_{231}a_1a_3 + \nu\lambda_2 a_2 &= -H_2/\lambda_2 \\ \dot{a}_3 + [(\lambda_2-\lambda_1)/\lambda_3]D_{231}a_1a_2 + \nu\lambda_3 a_3 &= -H_3/\lambda_3 \end{aligned}\right\}, \tag{2.7}$$

where $D_{231} = -8l/15\pi^2$ and ν is taken to be 0.01 (see Appendix A). This minimum system (2.7) is formally and philosophically the same as that studied by Lorenz (1960), but contains the additional forcing and dissipative terms. This severe truncation has the unfortunate consequence that the beta-effect is eliminated and the disturbances are phase-locked. In order to retain the beta-effect, we would have to include the cosine and sine terms corresponding to the two disturbance components in (2.6), and then we would have to face more complex algebra to determine the solutions and more difficult geometry of the solution surfaces in a five-component model.

As a first approach to studying the implications of the nonlinearity and the consequent multiple solutions in a forced flow, it therefore seems preferable to retain the maximum simplification model. Moreover, this elucidates the essential characteristics of the nonlinear term in producing multiple solutions.

Owing to the forcing by the Fourier coefficients H_n of the heating field, the equations are inhomogeneous and $a_1=a_2=a_3=0$ is not a solution, in accordance with Jeffreys' theorem (Dutton, 1976b). As a matter of experience (rather than rigorous deduction), the inhomogeneity may be expected to produce catastrophes rather than simple bifurcations on the solution surfaces for a_1, a_2, a_3. Since we know at least one stationary solution $\mathbf{A}$ must exist, we can put $\mathbf{a}(t)=\mathbf{A}+\alpha(t)$, and then have the homogeneous equations

$$\left.\begin{aligned} \dot{\alpha}_1 &= \Lambda_1(\alpha_2\alpha_3 + A_2\alpha_3 + A_3\alpha_2) - \nu\lambda_1\alpha_1 \\ \dot{\alpha}_2 &= \Lambda_2(\alpha_1\alpha_3 + A_1\alpha_3 + A_3\alpha_1) - \nu\lambda_2\alpha_2 \\ \dot{\alpha}_3 &= \Lambda_3(\alpha_1\alpha_2 + A_1\alpha_2 + A_2\alpha_1) - \nu\lambda_3\alpha_3 \end{aligned}\right\}, \tag{2.8}$$

where the Λ's are defined by comparison with (2.7)

3. Stationary solutions

The stationary solutions are a crucial subclass of solutions to the spectral systems (2.5) or (2.7). They can be determined analytically as an algebraic function of the model parameters ν, λ_n and H_n. Besides their intrinsic value, the stationary solutions are the foundation for the investigation of the asymptotic properties of the temporally varying solutions of (2.7).

By choosing $\alpha(t)=0$, the spectral system (2.7) becomes

$$\left.\begin{aligned} \Lambda_1A_2A_3 - \nu\lambda_1A_1 &= H_1/\lambda_1 \\ \Lambda_2A_1A_3 - \nu\lambda_2A_2 &= H_2/\lambda_2 \\ \Lambda_3A_1A_2 - \nu\lambda_3A_3 &= H_3/\lambda_3 \end{aligned}\right\}, \tag{3.1}$$

We assume that A_1 is known to solve the last two equations, linear in A_2 and A_3. This is possible with Cramer's rule provided that

$$\nu^2\lambda_2\lambda_3 - \Lambda_2\Lambda_3A_1^2 \neq 0.$$

But inspection of (2.7) shows that

$$\Lambda_2\Lambda_3=(\lambda_1-\lambda_3)(\lambda_2-\lambda_1)D_{231}^2/\lambda_2\lambda_2<0$$

for $\lambda_3>\lambda_2>\lambda_1$, as will always be the case here. Thus, we obtain $A_i=A_i(A_1,H_2,H_3)$, $i=2, 3$, and on substituting these results in the first equation, we have a fifth-degree polynomial in A_1,

$$P(A_1)=A_1^5+p_4A_1^4+\cdots+p_0=0, \qquad (3.2)$$

that governs the stationary solution. The coefficients are listed in Appendix B. Since the coefficients are real, complex roots must occur in conjugate pairs. Hence there is always at least one real root for (3.2) and may be one, three, or five depending on the parameter values.

With $\lambda_1<\lambda_2<\lambda_3$, expressions for all real solutions of (3.2) are easily calculated from (3.1) for three cases, giving the following expressions for A_1:

$$1.\ A_1=-\frac{H_1}{\nu\lambda_1^2}, \quad \text{for} \quad H_2=0, \quad H_3=0, \qquad (3.3)$$

$$2.\ A_1=0, \quad \text{for} \quad H_1=0, \quad H_2=0, \qquad (3.4)$$

$$3.\ A_1=0, \quad \text{for} \quad H_1=0, \quad H_3=0, \qquad (3.5)$$

and

$$A_1=\pm\left\{\frac{(\nu\lambda_2\lambda_3)^2}{(\lambda_1-\lambda_3)(\lambda_2-\lambda_1)D_{231}^2}+\frac{\lambda_3[(\lambda_2-\lambda_1)(\lambda_3-\lambda_2)H_2^2]^{\frac{1}{2}}}{\lambda_1(\lambda_3-\lambda_1)(\lambda_2-\lambda_1)|D_{231}|}\right\}^{\frac{1}{2}},$$

$$\text{for} \quad H_1=0,\ H_3=0, \text{ and } |H_2|>\hat{H}_2. \qquad (3.6)$$

This last case represents an example of branching or bifurcation of the solutions. It is clear from (3.1) that $A_1=A_3=0$, $A_2=-H_2/\nu\lambda^2$ is always a solution for $H_1=H_3=0$. But when $|H_2|$ exceeds the critical value

$$\hat{H}_2=\frac{\lambda_1\lambda_2^2\lambda_3\nu^2}{|D_{231}|[(\lambda_2-\lambda_1)(\lambda_3-\lambda_2)]^{\frac{1}{2}}}, \qquad (3.7)$$

two more solutions given by (3.6) appear, as illustrated in Fig. 3.1, branching off from the basic solution. This critical value corresponds, via $\hat{A}_2=-\hat{H}_2/\nu\lambda_2^2$, to a meridional wind speed amplitude of $\hat{v}\approx 26$ m s^{-1} for $l=1$. We will discuss the implication of the bifurcation or stability of these stationary solutions in Section 4.

Analytic solutions of (3.2) are not presently known for more general forcing configurations; however, the boundaries on which bifurcation occurs may be precisely specified in the space of the forcing values (H_1,H_2,H_3) as those regions in which (3.2) has a triple root. This boundary is thus determined by the parameters that give simultaneous solutions of $P(A_1)=0$, $P'(A_1)=0$, $P''(A_1)=0$. For the present case, bifurcation occurs only at $H_1=H_3=0$, $H_2=\hat{H}_2$. In bifurcation, three roots become a triple root at the bifurcation point. Another possibility is that two roots coalesce and then become complex. In this case, the remaining root is unaffected. The coalescence and disappearance of two roots is an example of a catastrophe and the set in the forcing space on which this occurs is given clearly by those parameters for which simultaneous solutions of $P(A_1)=0$, $P'(A_1)=0$ are possible. These two equations produced an analytic expression for the curves in (H_1,H_2) along which the number of roots changed. The numbers of roots in the various regions thus delineated were found with the aid of the Sturmian polynomial theory (Barnard and Child, 1936). The set of values (H_1,H_2) for which multiple stationary solutions exist is here called the morphogenesis set.

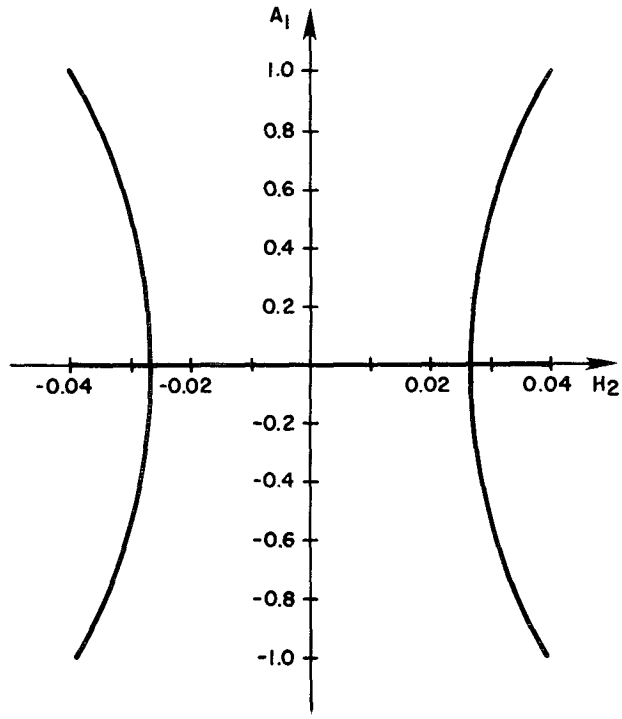

FIG. 3.1. The bifurcation diagram derived from (3.2) for $H_1=0$ and $H_3=0$. The trivial solution shown for H_2 in $(-0.04, 0.04)$ exists for all H_2. The critical values are ± 0.026.

Fig. 3.2 shows the arrangement of roots for $H_3=0$ in (3.1). The significance of the curve $q_2q_1=q_0$ and the stability of these solutions are addressed in Section 4. Application of Sturm's theorem (Barnard and Child, 1936, pp. 448–453) to points in the two regions of Fig. 3.2 separated by the curve $q_0=0$ demonstrates that Eq. (3.2) has three real roots for (H_1,H_2)-pairs inside the curve $q_0=0$, while in the region outside of $q_0=0$, only one real solution exists.

The reason for choosing $H_3=0$ is that the solutions of (3.2) in the form $A_1=A_1(H_2,H_3)$ can be explicitly portrayed in three-space. A numerical iteration scheme

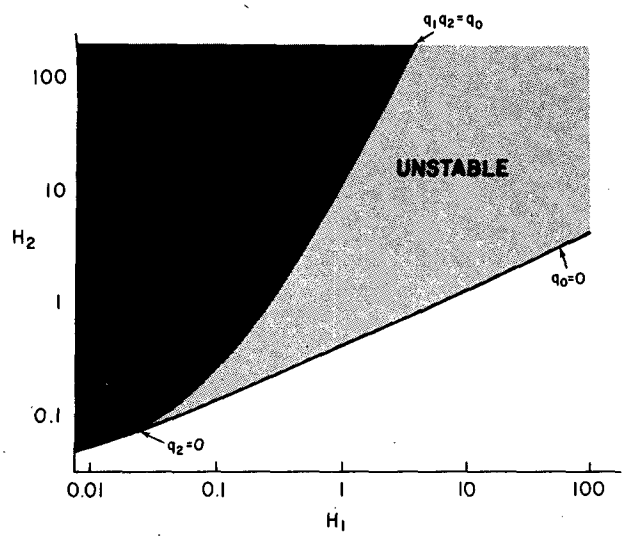

FIG. 3.2. Morphogenesis set derived from (3.2) for the cusp catastrophe ($H_3=0$), depicted in logarithmic coordinates. In the region to the left of the curve $q_0=0$, Eq. (3.2) has three real solutions. On $q_0=0$, (3.2) has a double root (two distinct solutions) and to the right of $q_0=0$, (3.2) has a unique real solution. The local stability, including the curve $q_1q_2=q_0$, is discussed in Section 4.

based on the fixed-point theorem was used to obtain the results shown in Fig. 3.3. The solution surface exhibits the characteristic form known as the cusp catastrophe.

The canonical equation for the cusp catastrophe is $x^3-bx-a=0$, with the parameters a and b. Numerical results confirm the conclusions from Sturmian theory shown in Fig. 3.3 that the quintic factors into a quadratic with conjugate roots and a cubic that is close enough to this form to exhibit the cusp form.

The situation is more complicated when all three heating parameters are allowed to vary. It is evidently impossible to portray $A_1=A_1(H_1,H_2,H_3)$ in one graph. We can take sections, as we did with $A_1=A_1(H_1,H_2,0)$ to find the cusp catastrophe or we can identify regions with fixed numbers of roots or stability properties in the control or parameter space (H_1,H_2,H_3). The result for numbers of roots is shown in schematic form in Fig. 3.4. Here the canonical form is $x^5-dx^3-cx^2-bx-a=0$, and the surface is known as a butterfly catastrophe. In our case, we are in effect holding one parameter constant and plotting against H_1,H_2,H_3, rather than against

$$a=p_0(H_1,H_2,H_3)/p_5,\ldots,\quad d=-p_4(H_1,H_2,H_3)/p_5.$$

Thus we have effected a (presumably complicated) coordinate transformation between the butterfly and the form shown in Fig. 3.4.

4. Stability

In this section, we consider the stability properties of solutions of the perturbation equations (2.8) with respect to the stationary solutions **A** for the cusp catastrophe.

a. *Local stability*

The system (2.8) is of the form

$$\dot{\boldsymbol{\alpha}}(t)+\mathbf{F}(\mathbf{A},\boldsymbol{\alpha})=0, \tag{4.1}$$

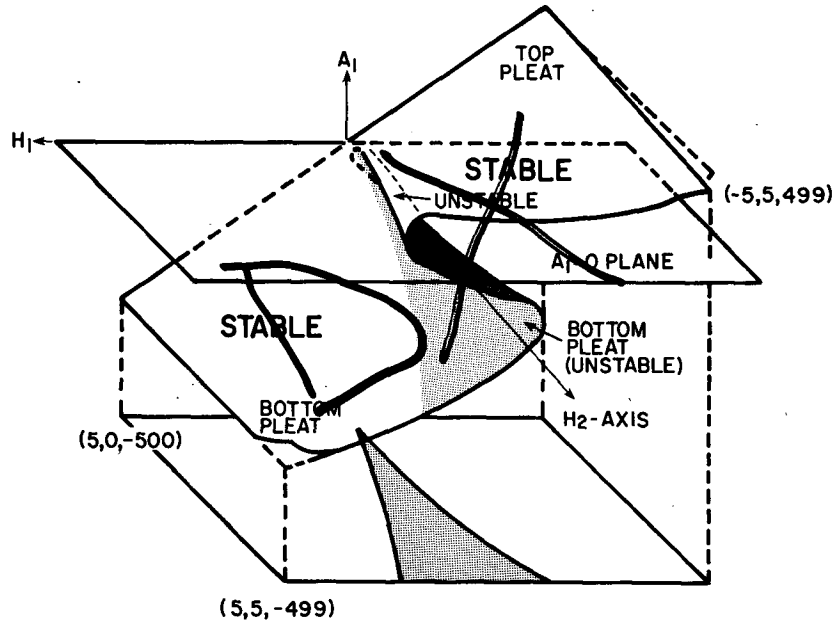

FIG. 3.3. The cusp catastrophe surface for solutions A_1 corresponding to the morphogenesis set of Fig. 3.2.

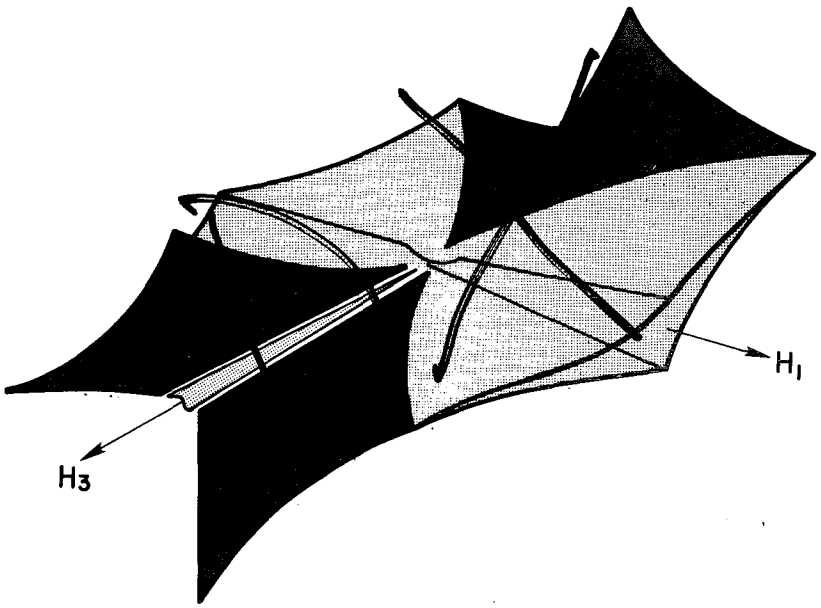

FIG. 3.4. Part of the morphogenesis set for the solutions of (3.2) for heating H_1,H_2,H_3; the vertical H_2 axis is not shown explicitly. The dark region indicates heating triples for which there are five solutions A_1, the shaded region has one solution and the white region has three. The dark and the shaded regions extend along the $\pm H_3$ axis indefinitely.

and as usual the local stability of (2.8) at $\mathbf{A}$ is examined by linearizing the operator $\mathbf{F}$ at $\mathbf{A}$. This is accomplished by ignoring products of perturbations, or more formally, by computing the linear matrix operator

$$\mathbf{L}_\mathbf{A}=\left\{\frac{\partial F_i}{\partial \alpha_j}\bigg|_{\alpha=0}\right\},$$

so that

$$\mathbf{F}(\mathbf{A}+\mathbf{h})-\mathbf{F}(\mathbf{A})=\mathbf{L}_\mathbf{A}\mathbf{h}+\mathbf{R}_\mathbf{A}(\mathbf{h}),$$

where $|\mathbf{R}_\mathbf{A}(\mathbf{h})|\,|\mathbf{h}|^{-1}$ vanishes as $|\mathbf{h}|$ does. The linearized equation is now

$$\dot{\boldsymbol{\alpha}}(t)+\mathbf{L}_\mathbf{A}(\boldsymbol{\alpha})=0. \tag{4.2}$$

Since (4.2) has solutions of the form $\boldsymbol{\alpha}(t)=\hat{\boldsymbol{\alpha}}e^{\sigma t}$, we obtain the characteristic equation

$$\sigma^3+q_2\sigma^2+q_1\sigma+q_0=0, \tag{4.3}$$

for the q_i defined in Appendix C. Hence, the linear stability of $\mathbf{A}$ to a perturbation $\boldsymbol{\alpha}(t)$ requires $\mathrm{Re}\{\sigma\}<0$ for each root σ.

Along the H_1 and H_3 axes, the stationary solutions are found with the aid of (3.3), (3.4) and Cramer's rule to be

$$\mathbf{A}=\left(-\frac{H_1}{\nu\lambda_1{}^2},\,0,\,0\right), \tag{4.4}$$

$$\mathbf{A}=\left(0,\,0,\,-\frac{H_3}{\nu\lambda_3{}^2}\right), \tag{4.5}$$

respectively. From (3.5), the unique stationary solution along the H_2 axis for $|H_2|<\hat{H}_2$ is

$$\mathbf{A}=\left(0,\,-\frac{H_2}{\nu\lambda_2{}^2},\,0\right). \tag{4.6}$$

For $|H_2|\gtrless\hat{H}_2$, we have this same solution along with the pair given in (3.6), where A_2 and A_3 are to be determined from Cramer's rule.

The three roots of (4.3) with $\mathbf{A}$ defined by any of (4.4)–(4.6) are

$$\sigma_1=-\nu\lambda_i, \tag{4.7}$$

$$\sigma_{2,3}=-\tfrac{1}{2}(q_2-\nu\lambda_i)\pm\tfrac{1}{2}[(q_2-\nu\lambda_i)^2-4q_0/\nu\lambda_i]^{\frac{1}{2}}, \tag{4.8}$$

where $i=1,2,3$ in both (4.7) and (4.8). The root (4.7) is real and negative.

From Appendix C, for $\lambda_1<\lambda_2<\lambda_3$ we see that q_0 is positive for $\mathbf{H}=(H_1,0,0)$ [$\mathbf{A}$ defined by (4.4)] and $\mathbf{H}=(0,0,H_3)$ with [$\mathbf{A}$ defined by (8.5)], so that for these two cases the real parts of (4.8) are negative. It follows that we have local stability for purely zonal forcing H_1 or for purely disturbance forcing H_3.

With forcing present in only the H_2 component, there are two cases. For $|H_2|<\hat{H}_2$ we note that $q_0>0$ for $\lambda_1<\lambda_2<\lambda_3$ with

$$\lim_{|H_2|\to\hat{H}_2} q_0=0.$$

Thus, in analogy with the previous H_1 and H_3 cases, the unique stationary solution (4.6) is locally stable. But when $|H_2|>\hat{H}_2$, one root in (4.8) is positive since

$q_0<0$. Therefore, we have demonstrated local instability of the solution (4.6) when $|H_2|>\hat{H}_2$.

Additionally, it may be demonstrated that the solution branches (3.6) are locally stable (Fig. 3.1) near the bifurcation point.

Finally, we discuss the local stability of the cusp morphogenesis set (Figs. 3.2 and 3.3) as determined with the aid of numerical computations. The edge of the cusp corresponds to $q_0=0$ in (4.3). To the right of $q_0=0$ in Fig. 3.2, the only real solution of Eq. (3.2) is locally stable. In the region between the curves $q_0=0$ and $q_1q_2=q_0$, Eq. (3.2) has three real solutions of which two are locally unstable. The region to the left of $q_1q_2=q_0$ is an area of two locally stable solutions and one unstable solution.

Along the curve $q_1q_2=q_0$, Eq. (4.3) has two imaginary solutions $\pm\sigma_I$ so that a Hopf bifurcation to periodic solutions of (2.8) with period $2\pi/|\sigma_I|\approx 53$ days may be expected for choices of heating rates near those given by $q_1q_2=q_0$ (Marsden and McCracken, 1976).

From local stability theory, we therefore have the following properties of the cusp catastrophe surface.

The curve $q_0=0$ in which one root of (4.3) vanishes delineates a stability transition and also the cusp or region of nonunique solutions. In the cusp, which contains the bifurcation (H_2) axis, the middle pleat ($|A_1|\approx 0$) is inaccessible because it is locally unstable (one positive $\mathrm{Re}\{\sigma\}$). The solutions on the top and bottom pleats become less stable as they approach the cusp and they become unstable (two $\mathrm{Re}\{\sigma\}>0$) after crossing $q_1q_2=q_0$.

Since the curve $q_1q_2=q_0$ does not coincide with the bifurcation axis, the cusp catastrophe model exhibits hysteresis. Thus, for forcing configurations to the left of $q_1q_2=q_0$ where both the bottom and top pleats are stable, we are confronted with divergence of solutions since small changes in the initial conditions may result in either a stable solution in which $|A_1|$ is small or a stable solution corresponding to $|A_1|$ large.

b. Global stability

The perturbation energy equation is found for the expansion (2.6) from (2.8) to be

$$\dot{E}(t)=\sum_{n=1}^{3}\lambda_n\alpha_n(t)\dot{\alpha}_n(t) \tag{4.10}$$

or

$$\dot{E}(t)=-\lambda_1\Lambda_1A_1\alpha_2\alpha_3-\lambda_2\Lambda_2A_2\alpha_1\alpha_3 -\lambda_3\Lambda_3A_3\alpha_1\alpha_2-\sum_{n=1}^{3}(\delta_i\alpha_i)^2, \tag{4.11}$$

in which Λ_i and $\delta_i=\sqrt{\nu}\lambda_i$ are defined by comparison with (2.8) and (4.10), and in which we have used $\sum_i\lambda_i\Lambda_i=0$.

In order to convert (4.11) into a form in which the sign may be determined more readily, we write it as ($\gamma_i=-\lambda_i\Lambda_i$) to obtain

$$\begin{aligned}\dot{E}(t)=&-\left(\delta_1\alpha_1-\frac{\gamma_3}{2\delta_1}A_3\alpha_2-\frac{\gamma_2}{2\delta_1}A_2\alpha_3\right)^2\\ &-\left\{\left[\delta_2^2-\left(\frac{\gamma_3A_3}{2\delta_1}\right)^2\right]^{\frac{1}{2}}\alpha_2-\frac{\left(\gamma_1A_1+\dfrac{\gamma_2\gamma_3}{2\delta_1^2}A_2A_3\right)}{2\left[\delta_2^2-\left(\dfrac{\gamma_3A_3}{2\delta_1}\right)^2\right]^{\frac{1}{2}}}\alpha_3\right\}^2\\ &-\left\{\delta_3^2-\left(\frac{\gamma_2A_2}{2\delta_1}\right)^2-\frac{\left(\gamma_1A_1+\dfrac{\gamma_2\gamma_3}{2\delta_1^2}A_2A_3\right)^2}{4\left[\delta_2^2-\left(\dfrac{\gamma_3A_3}{2\delta_1}\right)^2\right]}\right\}\alpha_3^2.\end{aligned} \tag{4.12}$$

Since $E(t)>0$ for nonzero perturbations, a necessary and sufficient condition for global, uniform, equiasymptotic stability of solutions of (2.8) (Cesari, 1971) is $\dot{E}(t)<0$. Clearly, this will obtain for A_1, A_2 and A_3 small enough. More precisely, the sufficient conditions for $\dot{E}<0$ are

$$\nu\lambda_3^2\geqslant\left[D_{231}\frac{(\lambda_3-\lambda_1)}{2\sqrt{\nu}\lambda_1}A_2\right]^2+\frac{\left\{-D_{231}(\lambda_3-\lambda_2)A_1-D_{231}^2\left[\dfrac{(\lambda_2-\lambda_1)(\lambda_3-\lambda_1)}{2\nu\lambda_1^2}\right]A_2A_3\right\}^2}{4\left[\nu\lambda_2^2-D_{231}^2\dfrac{(\lambda_2-\lambda_1)^2}{4\nu\lambda_1^2}A_3^2\right]}, \tag{4.13}$$

$$\delta_2^2>\left(\frac{\gamma_3A_3}{2\delta_1}\right)^2,$$

since then the coefficient of α_3^2 in the third term is non-negative.

Therefore, we have (for $\lambda_1<\lambda_2<\lambda_3$) global stability in the sense of Lyapunov along the H_1, H_2 or H_3 axes if

$$|H_1|<\frac{2(\nu\lambda_1)^2\lambda_2\lambda_3}{|D_{231}|(\lambda_3-\lambda_2)},\qquad H_2=0,\ H_3=0, \tag{4.14}$$

$$|H_2|<\frac{2(\nu\lambda_2)^2\lambda_1\lambda_3}{|D_{231}|(\lambda_3-\lambda_1)}=\overset{*}{H}_2,\quad H_1=H_3=A_1=0, \tag{4.15}$$

$$|H_3|<\frac{2(\nu\lambda_3)^2\lambda_1\lambda_2}{|D_{231}|(\lambda_2-\lambda_1)},\qquad H_1=H_2=0. \tag{4.16}$$

Because $\overset{*}{H}_2<\hat{H}_2$, global stability may not extend to the bifurcation point.

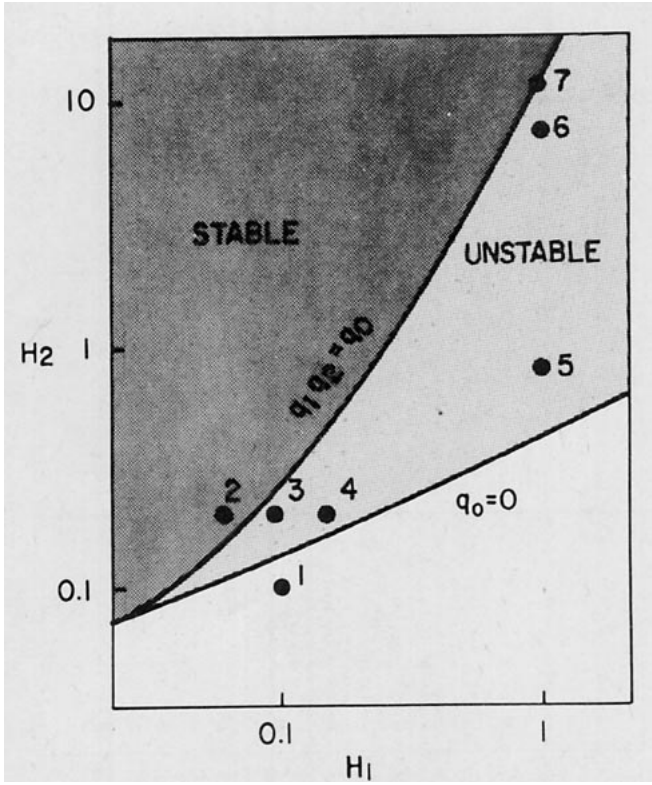

FIG. 4.0. Approximate location of initial values for the trajectories shown in Figs. 4.1–4.7, the figure number corresponding to the number shown above.

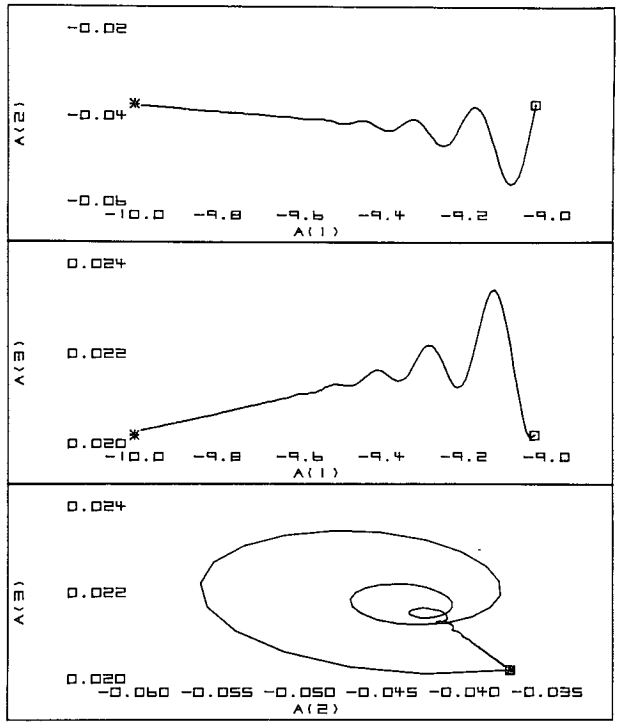

FIG. 4.1. Projection of the three-dimensional trajectory of the amplitude coefficients into the three phase planes for the initial values indicated by 1 in Fig. 4.0. The trajectories were obtained by numerical integration of (2.6) with $H_3=0$. Initial conditions are denoted by a box, while stationary points of the top pleat of Fig. 3.3 are indicated with an asterisk.

c. Numerical integrations

Trajectories derived by numerical integration of (2.7) (with $H_3=0$) for initial conditions near the cusp catastrophe surface (Fig. 3.3) are depicted in Figs. 4.1–4.7 for the locations shown on Fig. 4.0. Numerical integrations were continued for nearly 300 days in Figs. 4.1–4.5 and for 1000 days in Figs. 4.6 and 4.7. In each figure, the three-dimensional trajectory is depicted by showing projections on the three phase planes. The initial condition is indicated by $t=0$. An asterisk marks the projection of the stationary solution $\mathbf{A}_T$ of the top pleat (Fig. 3.3) in each phase plane (except in Fig. 4.1 where the stationary solution $\mathbf{A}_B$ lies on the bottom pleat). The trajectories chosen for illustration in the figures are representative of numerous trajectories obtained for other initial conditions.

In Fig. (4.1), the forcing configuration $\mathbf{H}=(H_1,H_2)$ is not an element of the cusp morphogenesis set (Fig. 3.2); so, there is a unique stationary solution of Eq. (2.7). This stationary solution is stable (one real $\sigma<0$ and negative real parts of both complex σ's), and the trajectory indicates that the stability is asymptotic.

The remaining figures depict trajectories resulting from H_1,H_2-pairs contained in the morphogenesis set. The indicated stationary solution $\mathbf{A}_T$ on the top pleat is accompanied by an unstable (three real σ's: one

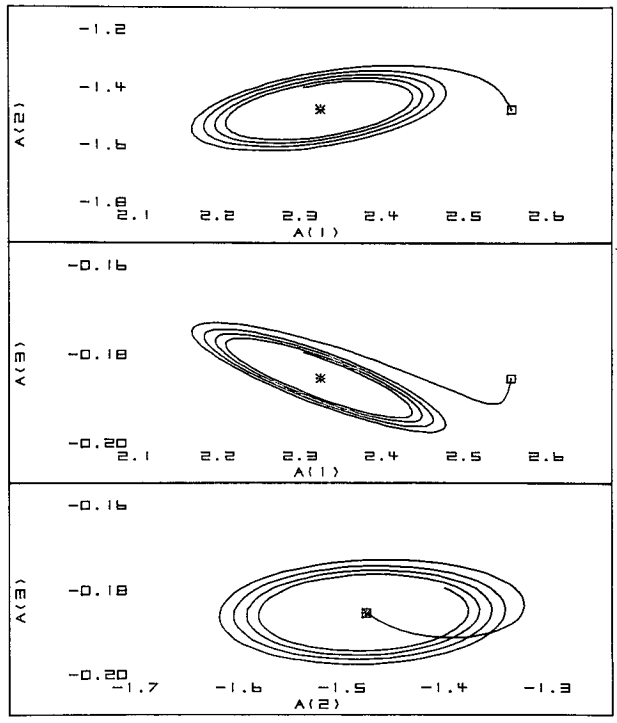

FIG. 4.2. Trajectory for initial point at 2 on Fig. 4.0.

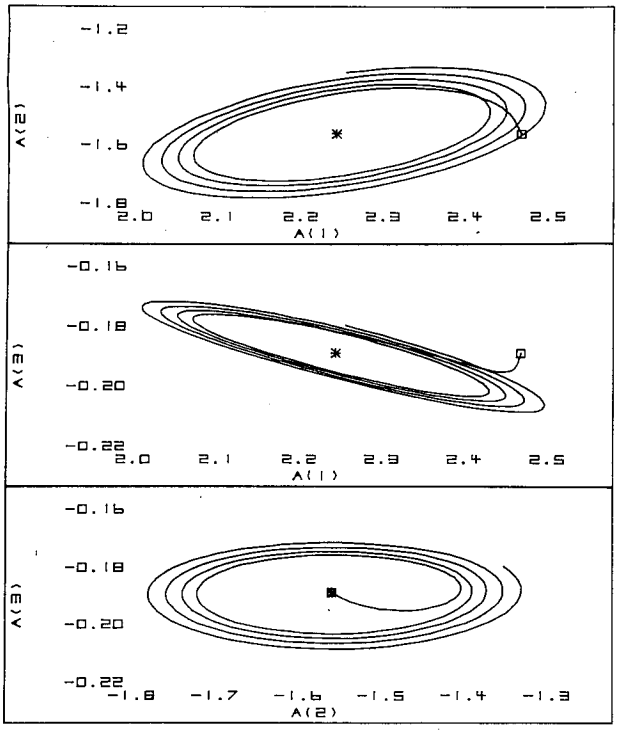

FIG. 4.3. As in Fig. 4.2 except at 3 on Fig. 4.0.

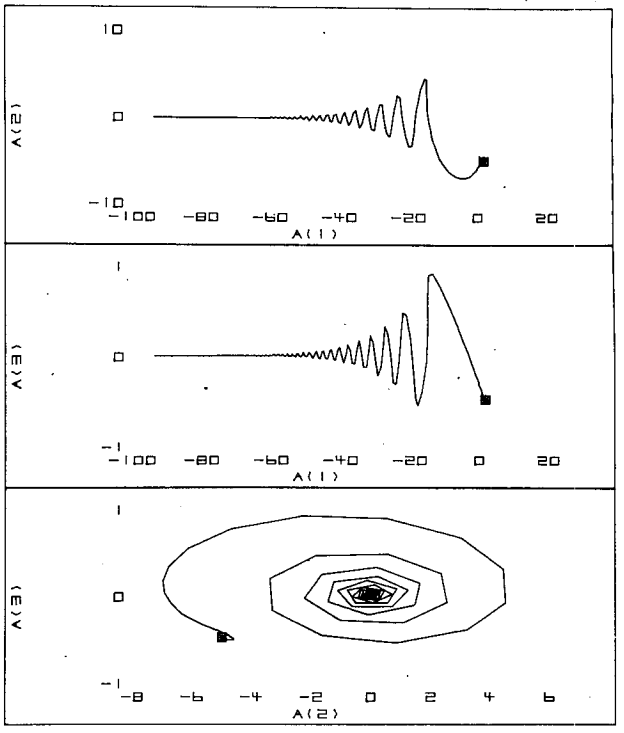

FIG. 4.5. As in Fig. 4.2 except at 5 on Fig. 4.0.

$\sigma>0$) stationary solution $\mathbf{A}_M$ on the middle pleat and a stable $\mathbf{A}_B$ on the bottom pleat.

The value of $\mathbf{H}$ chosen for Fig. 4.2 is near to and on the stable side of the curve $q_1q_2=q_0$. In agreement with the linear stability theory, the trajectory approaches $\mathbf{A}_T$ as $t\to\infty$.

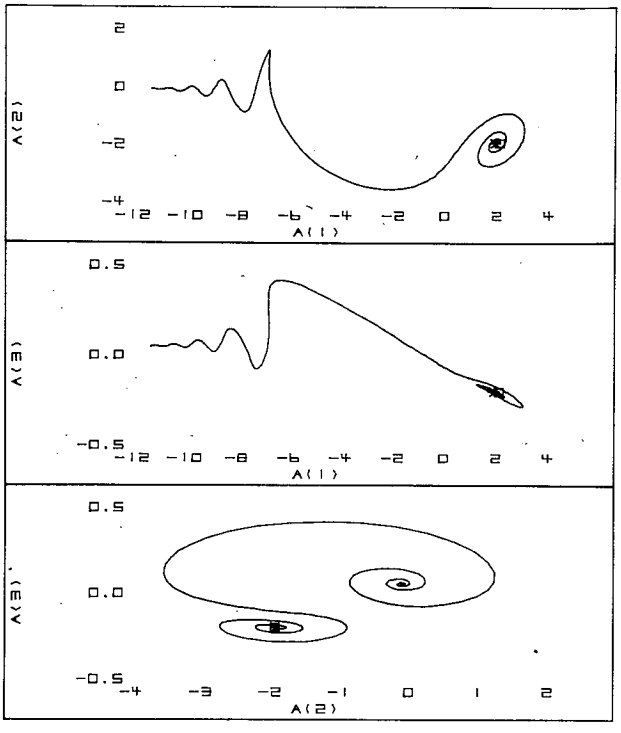

FIG. 4.4. As in Fig. 4.2 except at 4 on Fig. 4.0.

An unstable forcing configuration near $q_1q_2=q_0$ (one negative real and a complex σ-pair with positive real parts) is used for Fig. 4.3 and results in a trajectory that spirals away from $\mathbf{A}_T$.

As we approach the curve $q_0=0$ (Fig. 4.4) note that the rate of departure from $\mathbf{A}_T$ increases so that near $q_0=0$ (three real σ's: two positive, one negative) in Fig. 4.5, there is no perceptible oscillation in the zonal (a_1) component, and the trajectory quickly approaches the stable solution $\mathbf{A}_B$.

In Fig. 4.6, $\mathbf{H}$ is chosen to be near $q_1q_2=q_0$ on the unstable side. For the initial 80 days, this trajectory spirals from $\mathbf{A}_T$ in a manner similar to the trajectory of Fig. 4.3. However, by day 125 the trajectory has undergone a transition to a nearly periodic solution which persists throughout the integration interval ($t=1000$ days).

The behavior apparent in Fig. 4.6 leads us to postulate the existence of a transition region between $q_1q_2=q_0$ and $q_0=0$. To the left of the hypothetical region (on the $q_1q_2=q_0$ side), solutions of Eq. (2.7) exhibit, for numerical integrations of sufficient duration, the behavior characterized by the trajectory of Fig. 4.6. For H in the region to the right of this region (near $q_0=0$), Figs. 4.4 and 4.5 serve as models for the trajectories.

The forcing values (H_1,H_2) for Fig. 4.7 lie on the curve $q_1q_2=q_0$, along which the cubic equation (4.3)

has one real, negative root and two imaginary roots $\pm i\sigma_I$. Thus $q_1q_2=q_0$ is a curve along which we might expect a Hopf bifurcation to a periodic solution with period $2\pi/\sigma_I$. The trajectory in Fig. 4.7 is apparently approaching a limit cycle, and the apparent period is approximately $2\pi/\sigma_I$. But the limit cycle shown in Fig. 4.7 should not be the Hopf solution, which for the (H_1,H_2) values on $q_1q_2=q_0$ would have a zero amplitude.

The suggestion made by these results is that there are periodic or nearly periodic trajectories in the neighborhood of the Hopf solution that inherit some properties from it. The situation, as now recognized in theoretical work on bifurcating periodic solutions, suggests a subcritical bifurcation to a periodic solution (of "snap-through" type) and would appear to merit further investigation.

5. Conclusions

The stationary and evolutionary solutions of a three-component spectral model of forced, dissipative, nonlinear quasi-geostrophic flow have been examined for the case in which a zonal flow interacts with smaller scale disturbances.

A major consequence of adding heating and dissipation is that the structure of the solution set becomes quite complex; Lorenz (1960) showed that the equivalent unheated, inviscid model has strictly periodic solutions expressible as elliptic functions. Here we have instead the possibility of multiple stationary solutions with varying stability and domains of attraction or repulsion. Bifurcations and catastrophes occur in the model as the heating rates are varied. The obvious implication is that even more complex behavior can be expected in less severely truncated and temporally dependent models of atmospheric flow. Moreover, the hysteresis and divergence of solutions on the cusp catastrophe surface show that a successful theory of atmospheric climate will have to contend with multiple solutions, changing domains of attraction and intransitivity of the flow as external parameters are varied.

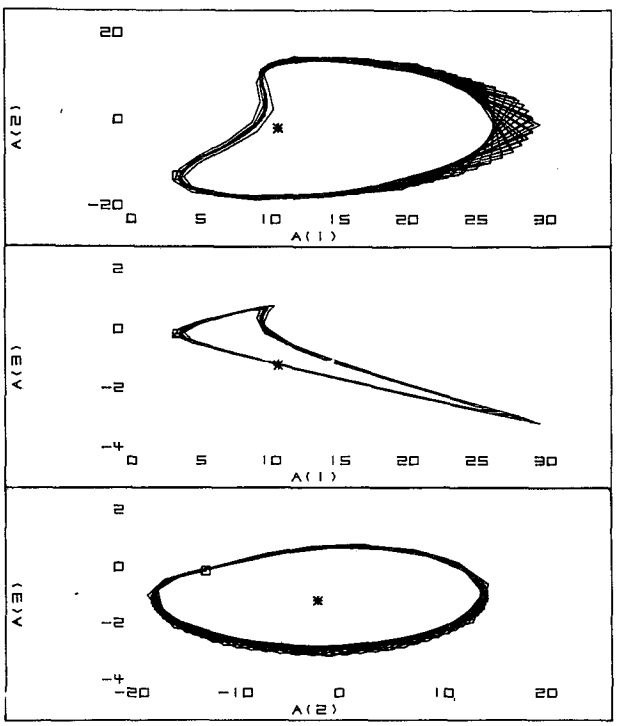

FIG. 4.6. As in Fig. 4.2 except at 6 on Fig. 4.0.

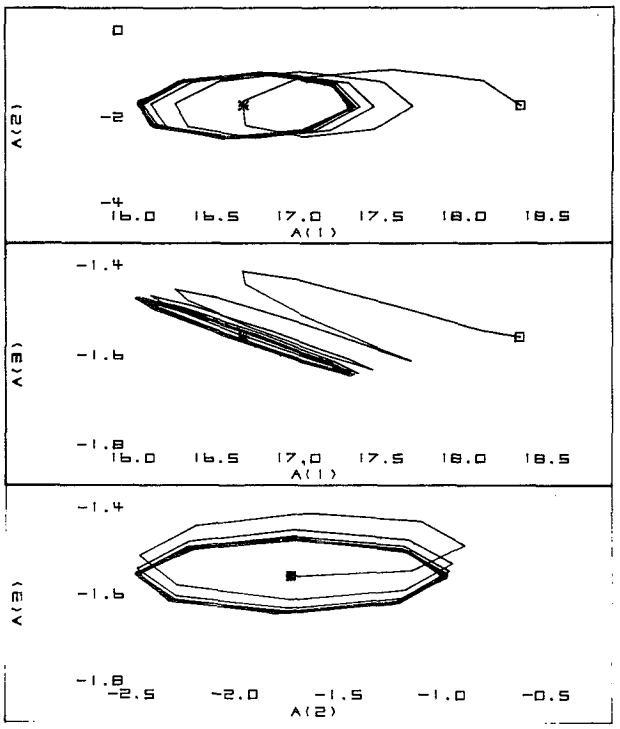

FIG. 4.7. As in Fig. 4.2 except at 7 on Fig. 4.0.

Acknowledgment. The research reported here was sponsored by National Science Foundation under Grant ATM73-00662-A03. We are indebted to H. N. Shirer for his interest and assistance.

APPENDIX A

Eddy Viscosity and Scales

The choice of an eddy viscosity coefficient is crucial in attempting to relate models such as the one studied here to atmospheric behavior. To arrive at the estimate used here we take the average dissipation as $D=6$ W m^{-2} and then write

$$D=\nu\int_0^\infty \rho|\nabla\mathbf{v}|^2dz,$$

so that

$$\nu_i=\frac{D}{p_0/g}\left(\frac{\Delta v}{\Delta x_i}\right)^{-2}.$$

For vertical shear dominant and with value $\Delta v/\Delta z = 20$ m s$^{-1}/10^4$ m, we have $\nu_3=1.5\times10^6$ cm^2 s^{-1}; for horizontal shear only with $\Delta v/\Delta x=20$ m s$^{-1}/10^6$ m, we obtain $\nu_H=1.5\ 10^{10}$ cm^2 s^{-1}.

The nondimensional value of ν in the present model is $\nu=\nu_H T/L^2$, so that we can choose $\nu=0.01$, $T=1$ day and $L=3.6\ 10^6$ m. Thus a nondimensional velocity $v=1.0$ corresponds to a dimensional velocity of approximately 40 m s^{-1}.

APPENDIX B

Coefficients of the Polynomial Eq. (3.2)

Eq. (3.2), which defines A_1, is of the form

$$A_1{}^5+p_4A_1{}^4+p_3A_1{}^3+p_2A_1{}^2+p_1A_1+p_0=0.$$

The coefficients p_i are as follows:

$$p_4=\frac{H_1}{\nu\lambda_1{}^2},$$

$$p_3=-\frac{2(\nu\lambda_2\lambda_3)^2}{(\lambda_1-\lambda_3)(\lambda_2-\lambda_1)D_{231}^2},$$

$$p_2=\frac{2H_1\nu(\lambda_2\lambda_3)^2}{\lambda_1{}^2(\lambda_3-\lambda_1)(\lambda_2-\lambda_1)D_{231}^2}-\frac{(\lambda_3-\lambda_2)H_2H_3}{\nu\lambda_1{}^2(\lambda_3-\lambda_1)(\lambda_2-\lambda_1)D_{231}},$$

$$p_1=\frac{(\nu\lambda_2\lambda_3)^4}{(\lambda_2-\lambda_1)^2(\lambda_2-\lambda_1)^2D_{231}^4}-\frac{(\lambda_3-\lambda_2)[(\lambda_1-\lambda_3)(\lambda_2H_3)^2+(\lambda_2-\lambda_1)(\lambda_3H_2)^2]}{\lambda_1{}^2(\lambda_3-\lambda_1)^2(\lambda_2-\lambda_1)^2D_{231}^2},$$

$$p_0=\frac{H_1\nu^3(\lambda_2\lambda_3)^4}{\lambda_1{}^2(\lambda_3-\lambda_1)^2(\lambda_2-\lambda_1)^2D_{231}^4}+\frac{(\lambda_3-\lambda_2)H_2H_3\nu(\lambda_2\lambda_3)^2}{\lambda_1{}^2(\lambda_3-\lambda_1)^2(\lambda_2-\lambda_1)^2D_{231}^3}.$$

APPENDIX C

Coefficients of the Characteristic Eq. (4.3)

The coefficients of (4.3) are

$$q_2=\nu(\lambda_1+\lambda_2+\lambda_3),$$

$$q_1=\nu^2(\lambda_1\lambda_2+\lambda_1\lambda_3+\lambda_2\lambda_3)-D_{231}^2\left[\frac{(\lambda_1-\lambda_3)(\lambda_2-\lambda_1)}{\lambda_2\lambda_3}A_1{}^2+\frac{(\lambda_3-\lambda_2)(\lambda_2-\lambda_1)}{\lambda_1\lambda_3}A_2{}^2+\frac{(\lambda_3-\lambda_2)(\lambda_1-\lambda_3)}{\lambda_1\lambda_2}A_3{}^2\right],$$

$$q_0=\nu^3\lambda_1\lambda_2\lambda_3+D_{231}^2\left\{\nu\left[\frac{(\lambda_3-\lambda_1)(\lambda_2-\lambda_1)}{\lambda_2\lambda_3}\lambda_1A_1{}^2-\frac{(\lambda_2-\lambda_1)(\lambda_3-\lambda_2)}{\lambda_1\lambda_3}\lambda_2A_2{}^2+\frac{(\lambda_3-\lambda_2)(\lambda_3-\lambda_1)}{\lambda_1\lambda_2}\lambda_3A_3{}^2\right]-2D_{231}\frac{(\lambda_2-\lambda_1)(\lambda_2-\lambda_1)(\lambda_3-\lambda_2)}{\lambda_1\lambda_2\lambda_3}A_1A_2A_3\right\}.$$

REFERENCES

Baer, F., 1970: Analytical solutions to low-order spectral systems. *Arch. Meteor. Geophys. Bioclim.*, **19**, 255–282.

Barnard, S., and J. M. Child, 1936: *Higher Algebra*. MacMillan and Co., 585 pp.

Cesari, L., 1971: *Asymptotic Behavior and Stability Problems in Ordinary Differential Equations*. Springer-Verlag, 271 pp.

Charney, J. G., 1947: The dynamics of long waves in a baroclinic westerly current. *J. Meteor.*, **4**, 135–162.

——, 1971: Geostrophic turbulence. *J. Atmos. Sci.*, **28**, 1087–1095.

Dickinson, R. E., 1969: Vertical propagation of planetary Rossby waves through an atmosphere with Newtonian cooling. *J. Geophys. Res.*, **74**, 929–938.

Dutton, J. A., 1974: The nonlinear quasi-geostrophic equation: Existence and uniqueness of solutions on a bounded domain. *J. Atmos. Sci.*, **31**, 422–433.

——, 1976a: The nonlinear quasi-geostrophic equation. Part II: Predictability, recurrence, and limit properties of thermally forced and unforced flows. *J. Atmos. Sci.*, **33**, 1431–1453.

——, 1976b: *The Ceaseless Wind: An Introduction to the Theory of Atmospheric Motion*. McGraw-Hill, 579 pp.

Fjørtoft, R., 1953: On the changes in the spectral distribution of kinetic energy for two-dimensional, nondivergent flow. *Tellus*, **5**, 225–230.

——, 1959: Some results concerning the distribution and total amount of kinetic energy in the atmosphere as a function of external heat sources and ground friction. *The Atmosphere and the Sea in Motion*, B. Bolin, Ed., Rockefeller Institute Press, 509 pp.

Lorenz, E. N., 1960: Maximum simplification of the dynamic equations. *Tellus*, **12**, 243–254.

——, 1973: Deterministic nonperiodic flow. *J. Atmos. Sci.*, **20**, 131–141.

Marsden, J. E., and M. McCracken, 1976: *The Hopf Bifurcation and Its Applications*. Springer-Verlag, 408 pp.

Phillips, N. A., 1954: Energy transformations and meridional circulations associated with simple baroclinic waves in a two-level, quasi-geostrophic model. *Tellus*, **6**, 273–386.

——, 1963: Geostrophic motion. *Rev. Geophys.*, **2**, 123–176.

Platzman, G. W., 1960: The spectral form of the vorticity equation. *J. Meteor.*, **17**, 635–644.

——, 1962: The analytical dynamics of the spectral vorticity equation. *J. Atmos. Sci.*, **19**, 313–328.

Stakgold, I., 1971: Branching of solutions of nonlinear equations. *SIAM Rev.*, **13**, 289–332.

Stone, P. H., 1972: A simplified radiative-dynamic model for the static stability of rotating atmospheres. *J. Atmos. Sci.*, **29**, 405–418.

Thom, R., 1976: *Structural Stability and Morphogenesis*. W. A. Benjamin, 339 pp.

Zeeman, E. C., 1976: Catastrophe theory. *Sci. Amer.*, **234**, 65–83.